Magneto-optical response of CdSe nanostructures

Pochung Chen and K. Birgitta Whaley
Department of Chemistry and Pitzer Center for Theoretical Chemistry, University of California, Berkeley, California 94720, USA
(Received 15 August 2003; revised manuscript received 14 January 2004; published 19 July 2004)

We present theoretical calculations of the Landé g factors of semiconductor nanostructures using a time-dependent empirical tight-binding method that allows a nonperturbative treatment of both the spin-orbit interaction and an external magnetic field. The electromagnetic field is incorporated into the tight-binding Hamiltonian in a gauge-invariant form. Eigenenergies and eigenfunctions of the band edge states are calculated as a function of the external magnetic field, and the g factors are then extracted from the field-induced energy splitting of the eigenstates. The size and aspect ratio dependence of both electron and hole g factors are investigated for CdSe nanostructures. We find that the electron g factors for single nanocrystals are weakly dependent on nanocrystal size and are strongly anisotropic, where the extent of anisotropy depends on the aspect ratio of the nanocrystal. The hole g factors are also anisotropic and are found to show more complex, oscillatory behavior as a function of size, due to a size-dependent mixing between the heavy hole-light hole components of the valence band edge states. The calculated electron g factor values are seen to be in good quantitative agreement with experimental measurements, suggesting that the multiple g factor values extracted from time resolved Faraday rotation experiments may be due to distinguishable components of the electron g factor tensor. Extension to the calculation of exciton g factors appears feasible with this approach.

DOI: 10.1103/PhysRevB.70.045311 PACS number(s): 73.22.−f, 73.21.La

I. INTRODUCTION

Spin dynamics in semiconductor nanostructures have been studied intensively in recent years, motivated by the emerging field of semiconductor spintronics and quantum information processing.[1] The most important time scale when implementing the quantum computer is the decoherence time of the quantum degree of freedom which is intended to be used as the qubit. Typically the spin decoherence time in the bulk semiconductor material is extremely short. However, it is expected that the spin decoherence time should increase substantially in nanostructures due to the three-dimensional quantum confinement. This expectation is supported by the optical orientation experiments of Gupta *et al.*[2] where a nanosecond spin lifetime was measured for neutral CdSe nanostructures. This indicates that there will be plenty of time to perform quantum operations on the spin degree of freedom in semiconductor nanostructure before the coherence is lost. Consequently, spins in nanostructures are excellent candidates for qubits. On the other hand, both spin based quantum computation and spintronics require precise control of the spin. Since the control of the spin dynamics in nanostructures is strongly dependent on the g factors of electrons, holes, and excitons in the nanostructure, it is imperative to understand the behavior and magnitude of g factors.

Experimentally the g factors of CdSe nanocrystals with wurtzite lattice structure have been measured via time resolved Faraday rotation (TRFR)[2,3] and magnetic circular dichroism (MCD).[4] The TRFR experimental measurements revealed multiple g factors. Two or four distinct g factor values were extracted, depending on the size of the nanostructure which ranged from ~22 to ~80 Å in diameter. The size distribution of the samples was estimated as 5%–15%.[3,5] Samples from ~22 to ~57 Å have a size-dependent mean aspect ratio that ranges from 1.0 to 1.3, with a ±0.2 variation.[3,5,6] In contrast to the TRFR measurements, MCD measurements (carried out for nanocrystals with 19 and 25 Å in diameter) reveal only a single exciton g factor.[4]

No definitive assignment of the multiple g factors measured in TRFR has been made. It was suggested in Ref. 2 that the lowest observed g factor be assigned to an isotropic electron g factor and all other g factors be assigned to excitonic states. It was also speculated there that exciton spin precession might only occur within a "quasispherical" regime where the expected anisotropy due to nanocrystal shape cancels the expected anisotropy due to the wurtzite crystal structure, resulting in an isotropic exciton g factor and thus reducing the overall number of observed g factors. These arguments were partially based on effective mass estimates for the g factors, with the hole contribution treated as a size-independent fitting parameter.[2] Recent perturbative calculations within a tight-binding description have shown a marked shape dependent anisotropy of the electron g factor[6] that would yield multiple g factors from the electron alone, as well as evidence for quasispherical regime for certain aspect ratio shapes. However, the perturbative nature of those calculations precluded a direct quantitative comparison with the experimentally measured g factors.

The hole spin is initially aligned by the optical pumping in a TRFR experiment. It has been argued that a fast decoherence of the hole spin nevertheless makes it impossible to detect the hole g factor in TRFR.[2] Unfortunately, the rate of hole decoherence in CdSe nanostructures is not known, with neither experimental measurements nor theoretical estimates available. While it is well established experimentally[8] and theoretically[9] that the hole spin decoherence time in the bulk semiconductor is extremely small, the three-dimensional quantum confinement might alter the hole spin decoherence time in a nanostructure. Recent time resolved photoluminescence on InAs/GaAs quantum dots[10] suggests that neither the electron nor the hole spin relax on the time scale of the lifetime of the exciton in this system. Although no estimation

of the hole relaxation time could be made, this does suggest that the hole decoherence time becomes much longer in nanoconfined systems. It is thus not yet clear whether the hole *g* factor signature should appear in a TRFR experiment, and the possibility of this should not be ruled out.

In theoretical work, the size dependence of the electron *g* factor in semiconductor nanostructures has been calculated within the eight band Kane model,[11–13] and within the tight-binding model using a perturbative approach.[6,14] In general, the effective mass approximation-type calculation is inadequate for nanostructures at small sizes ($\leqslant$30 Å) as the atomic nature and surface effects become more dominant in determining the details of the electronic states. Because of its atomistic nature, the tight-binding model is well suited to study the electronic and optical properties of nanostructures in this size range.

The results of the tight-binding study of Ref. 6 showed a strong shape dependence in the electron *g* factor. It was observed that a transition from anisotropic to isotropic electron *g* factor tensor occurs at aspect ratio $\approx$0.3, resulting in a quasispherical regime as originally suggested by Gupta and co-workers.[2] This previous tight-binding approach to calculation of *g* factors was based on Stone's formula[15] which is derived from a double second-order perturbation analysis in which both the spin-orbit interaction and the external magnetic field, i.e., all spin-dependent components of the electronic Hamiltonian, are treated perturbatively. As mentioned above, this perturbative analysis could not provide quantitatively accurate estimates of the magnitude of the *g* factors. This is not too surprising since the spin-orbit interaction is strong in CdSe (λ_{Cd}=0.151 eV and λ_{Se}=0.320 eV), and one therefore expects that this needs to be treated nonperturbatively in order to arrive at quantitatively accurate electron energy levels, whether in zero or finite magnetic field. Nonperturbative treatment of spin-orbit terms not only provides a more accurate estimation of the electron *g* factors for nanostructures with strong spin-orbit interaction, but also allows a systematic analysis of the hole and exciton *g* factors, in addition to the electron *g* factors.

It is also intriguing to investigate the possibility of a quasispherical regime within a more accurate calculation of the electron *g* factor than is afforded by the perturbative approach. In this paper, we find that with a nonperturbative treatment of both the spin-orbit and external magnetic field, the electron *g* factors are considerably more strongly anisotropic than was found with the perturbative analysis in Ref. 6 and the magnitude of the *g* factors is now in good agreement with the experimental measurements. This indicates that the effect of the spin-orbit interaction is too strong to be treated perturbatively when quantitatively accurate values of *g* factors are required.

This paper presents nonperturbative theoretical calculations of both the electron and hole *g* factors for CdSe nanostructures, employing a time-dependent implementation of empirical tight-binding theory. As mentioned above, both the spin-orbit interaction and the external magnetic field are taken into account nonperturbatively in this approach. The *g* factors are extracted from the magnetic field induced energy shifts of the electron and hole eigenvalues. We analyze the size and aspect ratio dependence of the electron and hole *g* factors for CdSe nanocrystals. We observe that the electron *g* factors show a weak monotonic decrease as a function of size and are strongly anisotropic. The magnitude of the calculated values agrees well with the experimental values extracted from TRFR measurements on CdSe nanocrystals of similar size and aspect ratio. We discuss the implications of this quantitative agreement and the extent to which the electron *g* factors can explain the TRFR experimental data. Detailed analysis indicates that the calculated electron *g* factors show a partial cancellation of anisotropy effects deriving from the wurtzite structure and from the aspect ratio. However, for these quantitatively accurate calculations, it appears that there is no size regime in which a complete cancellation corresponding to a quasispherical system would be obtained, in contrast to the previous expectations from effective mass[2] and the perturbative tight-binding approach.[6] The calculated hole *g* factors have very different behavior from that of the electrons, showing marked oscillations as a function of the size. This is shown to be a result of mixing between the heavy hole and light hole states, which is strongly dependent on the nanocrystal size. The present paper does not include direct calculation of exciton *g* factors. However, the same time-dependent approach can be easily extended to calculate an exciton *g* factor with the Coulomb interactions included nonperturbatively.[16,17]

The rest of the paper is organized as follows: In Sec. II we summarize the empirical tight-binding Hamiltonian for CdSe nanostructures and its solution in finite magnetic fields. We show that the time-dependent approach provides an efficient way to achieve the high energy resolution required to extract *g* factors from a finite field analysis. In Sec. III we present our numerical results for CdSe nanocrystals, including as reference points the total density of states and band gap, before presenting the electron and hole *g* factors that constitute the main focus of this work. In Sec. IV we summarize and draw conclusions from our results, and describe possible extensions to excitonic calculations.

II. THEORY AND DETAILS OF NUMERICAL CALCULATIONS

A. Tight-binding model of CdSe nanostructure

We start from the empirical tight-binding model for the bulk CdSe semiconductor with an sp_3s^* basis. The CdSe parameters for the wurtzite structure[18] are derived from the empirical parameters obtained by Lippens and Lannoo[19] for bulk CdSe in the zinc-blende structure, assuming nearest-neighbor interactions only. We construct the CdSe nanocrystals with wurtzite structure corresponding to the typical CdSe nanostructures seen in transmission electron microscopy images.[20] The constructed structures have approximate C_{3V} symmetry. The same structures have been used in previous time-independent tight-binding studies.[6,18,21] We remove the dangling bonds on the surface by shifting the energies of the corresponding hybrid orbitals well above the conduction band edge (by about 100 eV). The spin-orbit interaction is included in the zeroth order Hamiltonian.[21] Spin-orbit coupling constants are assigned to both types of atoms, with λ_{Cd}=0.151 eV and λ_{Se}=0.320 eV, respectively.[34] In order to

reproduce the *A*-*B* splitting within the sp_3s^* basis, a crystal field of −40 meV is added to the p_z local orbitals.[21]

B. Time-dependent approach to calculation of energy levels

We employ here a time-dependent approach to the calculation of the band edge energy states in zero and finite magnetic field. This method has been applied previously to the calculation of electronic properties of CdSe nanocrystals with zinc blende structure,[16] and to excitonic properties of Si nanocrystals.[22] It is a spectral evolution approach that is useful when the properties of a few states are required, e.g., states near the band edges, to very high accuracy and precision. When all eigenvalues and eigenvectors are required the time-dependent approach is computationally equivalent to direct diagonalization. One main advantage of the time-dependent approach for calculation of electronic properties of semiconductor nanostructures is the ability to efficiently incorporate electron-hole interactions, allowing straightforward calculation of excitonic energies in situations where the time-independent approach would require significantly more expensive calculations as a result of the increase in basis set size.[16] While efficient direct diagonalization methods for sparse matrices do allow high precision calculation of single electron states, as has recently been demonstrated with calculation of band edge states of InAs self-assembled quantum dots in finite magnetic fields, yielding electron and hole g factors,[23] extending such time-independent calculations to calculation of g factors for exciton states does not appear feasible at this time. In contrast, as we discuss below, the degree of precision afforded by the time-dependent approach to eigenenergy calculations in the finite field calculation of g factors should also be achievable for exciton states possessing electron-hole correlation.

The time-dependent method depends essentially on the spectral decomposition for an arbitrary initial state. Let $|E_n\rangle$ be the complete set of eigenfunctions of the Hamiltonian. Any initial state $|\psi(0)\rangle$ can be expressed as the linear combination of the eigenfunctions

$$|\psi(0)\rangle = \sum_n b_n |E_n\rangle. \tag{1}$$

The wave function at a later time t is

$$|\psi(t)\rangle = e^{-iHt}|\psi(0)\rangle = \sum_n b_n e^{-iE_n t}|E_n\rangle. \tag{2}$$

Projecting the wave function at time t onto the initial wave function and performing the Fourier transform one finds

$$\int_{-\infty}^{\infty} dt e^{iEt}\langle\psi(0)|\psi(t)\rangle = \sum_n |b_n|^2 \delta(E - E_n). \tag{3}$$

Thus the resulting Fourier spectrum can give us the spectral weight of the initial state in the eigenfunction basis and the eigenenergies of the eigenstates, provided that the eigenstates have nonzero overlap with the initial state. To get the total density of states one can sum over the spectral decompositions obtained using each wave function in a complete set as the initial state in term. The natural and convenient complete set to choose in the tight-binding framework is the direct product set of all local site orbitals, atomic orbitals, and spin states. Then

$$\sum_n \delta(E - E_n) = \sum_{i\ell\sigma} \int_{-\infty}^{\infty} dt e^{iEt}\langle\psi_{i\ell\sigma}(0)|\psi_{i\ell\sigma}(t)\rangle \tag{4}$$

where $|\psi_{il\sigma}(0)\rangle = |\text{site}, \text{orbital}, \text{spin}\rangle$. To achieve δ-function resolution one would need to have the infinite length record of the correlation function $\langle\psi(0)|\psi(t)\rangle$. In practice only a finite length T of record is available, which gives rise to artificial sidebands around a broadened δ-function approximation. The finite record length is taken into account by multiplying the right hand side of Eq. (4) with the normalized Hamming window function $w(t)$,[24] where

$$w(t) = 1 - \cos\left(\tfrac{2\pi t}{T}\right), \text{ if } 0 \leqslant t \leqslant T,$$

$$= 0, \text{ if } t > T. \tag{5}$$

The window function will reduce the sidelobes of the broadened δ functions and generate a normalized peak height. The resulting spectrum is of the form

$$\sum_n \mathcal{W}_n \mathcal{L}(E - E_n) = \sum_{i\ell\sigma} \int_0^{\infty} dt e^{iEt} w(t)\langle\psi_{i\ell\sigma}(0)|\psi_{i\ell\sigma}(t)\rangle, \tag{6}$$

where $\mathcal{W}_n$ represents the absolute spectral weight in eigenstate $|E_n\rangle$ and the line shape function $\mathcal{L}(E-E_n)$ is defined by

$$\mathcal{L}(E - E_n) = \frac{e^{i(E-E_n)T} - 1}{i(E - E_n)T} - \frac{1}{2}\sum_{s=\pm 1} \frac{e^{i(E-E_n)T + 2s\pi} - 1}{i(E - E_n)T + 2s\pi}. \tag{7}$$

If the total wave function propagation time is T, the energy resolution is $\sim\Delta E = \pi/T$. If the energy difference between the desired eigenenergy E_n, and adjacent eigenenergies, is larger than π/T, the spectrum near energy E_n can be approximately represented by $\mathcal{W}_n\mathcal{L}(E-E_n)$ with very high accuracy. Assuming this form, the value of the eigenvalue can be determined with accuracy much higher than π/T. To get the most accurate value possible it is desirable to perform the time integration of Eq. (6) by direct integration instead of using a discrete Fourier transform.

In order to use the spectral method one must be able to calculate the time propagator e^{-iHt} efficiently. In order to accomplish this we first break the time propagator into a series of short time propagators $e^{-iHt} = (e^{-iHdt})^N$ with $t = Ndt$. For the short time propagator we make use of the Baker-Hausdorff formula[25] to obtain the expansion

$$e^{-iHdt} = e^{-i(H_1 + \cdots + H_n)dt}$$

$$\approx e^{-iH_1 dt} \cdots e^{-iH_n dt} e^{-iH_n dt} \cdots e^{-iH_n dt} + O(dt^3). \tag{8}$$

To implement this decomposition we first break the tight-binding Hamiltonian into the on-site self-energy terms, the local spin-orbit terms, the local Zeeman terms, and the hopping terms. The on-site spin-orbit interaction is diagonalized and exponentiated analytically in the basis of the tight-binding orbitals, i.e., the 6×6 matrix of the p orbitals with spin. For the hopping terms we further use the checkerboard

decomposition[16,26] to divide these to different independent directions. Note that in the zinc blende structure there are only four fundamental directions while in the wurtzite structure there are seven fundamental directions. As a result of this decomposition each term contributing to the short time propagator can be consequently evaluated analytically[16] and the time evolution of the state can be calculated very efficiently.

The eigenfunction $|E_n\rangle$ with eigenenergy E_n can be calculated from

$$|E_n\rangle \propto \int_0^\infty dt e^{iE_n t}|\psi(t)\rangle, \tag{9}$$

provided there is nonzero overlap between the initial wave function and the desired eigenfunction, i.e., $\langle E_n|\psi(0)\rangle \neq 0$. Typically when there is no magnetic field ($\mathbf{B}=0$), the initial state is taken as a uniform superposition of local orbitals with specific angular momentum indices. The resultant eigenfunctions are then used as the starting point to calculate the eigenfunctions and eigenenergies when the magnetic field is turned on.

If there are degenerate eigenstates, the right hand side of Eq. (9) will in general be some unknown linear combination of these eigenstates. However, if a set of exact or approximate quantum numbers which can be used to label the degenerate eigenstates are known in advance, eigenfunctions corresponding to definite quantum numbers can be derived by judiciously choosing an initial state having the same quantum numbers. Typically the angular momentum index is used in this work for this purpose. This property will be used to generate Kramer's doublets in our calculations. More details of these procedures are given below and in Sec. III.

There are three important energy scales in this problem. The first energy scale is the energy difference between lowest conduction electron and higher energy conduction electrons and the difference between highest valence hole and lower energy hole states. This energy scale is typically at the order of 100 meV or larger. The second energy scale is the energy difference between nearly degenerate hole states that correspond approximately to the heavy-hole and light-hole states in the bulk limit. This energy scale is size dependent and is sensitive to the shape of the nanocrystals. In our calculation we find this energy scale to be 1–100 meV. The third important energy scale is the magnetic field induced splitting for a Kramer's doublet from which the g factors are extracted. Typically this energy scale ranges from a few to several hundred μeV.

The maximum total propagation time in the present calculations is about $1,280,000\ 1/\mathrm{eV}$, resulting in an energy resolution of 2.5 μeV. This energy resolution is enough to single out the spectrum of band edge electron and hole states from other higher energy states. It is also sufficient to resolve the two nearly degenerate hole states at the band edge. Once a high resolution eigenfunction is generated, by using window function Eqs. (5) and (6) to suppress the contribution from adjacent eigenstates, the eigenenergies of band edge states can be determined with accuracy up to 1 μeV. Since the accuracy is determined primarily by the total propagation time, we can expect to be able to achieve a similar accuracy for calculation of Zeeman shifts of excitonic states incorporating electron-hole correlation.

C. Calculation of the *g* factors

The g factors are obtained from a finite field analysis in which the electron and hole eigenvalues are calculated as a function of an applied external magnetic field. The full Hamiltonian is thus

$$H = H_0 + g_0\mu_B \mathbf{s}\cdot\mathbf{B} + \mu_B \mathbf{l}\cdot\mathbf{B}, \tag{10}$$

where H_0 is the tight-binding Hamiltonian including spin, i.e., incorporating all spin-orbit interactions,[17] $\mathbf{l}$ is the electron orbital angular momentum operator, and $\mathbf{s}$ the electron spin operator (g_0 is the free electron g factor, and μ_B the Bohr magneton). Noting that the spin-orbit coupling has already been incorporated in the zeroth order Hamiltonian as described above (in contrast to the perturbative analysis in Ref. 6), we shall refer to $\mathbf{B}$-dependent terms in Eq. (10) as the effective magnetic Hamiltonian, H_m, i.e., H_0+H_m.

When there is no external magnetic field ($\mathbf{B}=0$) Kramer's theorem guarantees that each eigenstate is at least twofold degenerate. In bulk CdSe the heavy hole and light hole are also degenerate at the Γ point. In a CdSe nanostructure it is expected that the quantum confinement will lift this degeneracy of heavy and light holes. Therefore, in this work the g factors obtained from finite field calculations will be defined with respect to the zero field Kramer's doublets. For a Kramer's doublet the effective magnetic Hamiltonian has the form

$$H_m(\mathbf{B}) = \mu_B \mathbf{B}\cdot\mathbf{G}\cdot\mathbf{S}, \tag{11}$$

where $\mathbf{S}$ is the effective spin operator which is defined with respect to the two Kramer's states $|\psi^{\pm}\rangle$, and $\mathbf{G}$ is the 3×3 g factor tensor. In the resulting basis of the Kramer's pairs, the effective spin operator $\mathbf{S}$ has the form

$$\mathbf{S}_x = \frac{m}{2}\sigma_x,\ \mathbf{S}_y = \frac{m}{2}\sigma_y,\ \mathbf{S}_z = \frac{m}{2}\sigma_z, \tag{12}$$

where m is an integer chosen so that the real spin $\mathbf{s}$ and effective spin $\mathbf{S}$ are approximately equal.

The eigenvectors of the $\mathbf{G}$ tensor define a principal axis frame for the twofold degenerate space spanned by the Kramer's doublet. It is important to clarify the definition and the sign convention for the g factors derived from such a finite field analysis, especially when these g factors are anisotropic. Let $\hat{e}_i$, $i=1, 2, 3$ be the principal axes. Then an external magnetic field

$$\mathbf{B} = B_1\hat{e}_1 + B_2\hat{e}_2 + B_3\hat{e}_3 \tag{13}$$

will give rise to a Zeeman splitting

$$\Delta E(\mathbf{B}) \equiv (E(\mathbf{B}) - E(0)) = \mu_B \sum_i g_i B_i. \tag{14}$$

We will denote the values g_i as principal g factors. Individual g_i can be identified by varying the external magnetic field $\mathbf{B}$ along each of the principal directions in turn and calculating the corresponding field dependent Zeeman splitting in each case.

In order to carry out these calculations, one needs to generate the eigenvectors of the **G** tensor within each Kramer's doublet. In a time-independent calculation, this would be done by making a degenerate perturbation theory analysis of the Kramer's doublets at zero field in order to find the correct basis for the effective spin **S** at a finite B field. Within the time-dependent approach we first generate initial zero-field states having definite total angular momentum indices $\mathbf{j}=\mathbf{s}+\mathbf{l}$ and j_z, and then calculate the corresponding Zeeman energy shift for these. We can verify that the initial state is a good zero-field eigenstate that evolves to the correct angular momentum basis for **S** at finite field by checking that the amplitude of the Zeeman-shifted spectral peak remains constant at finite **B**. Any substantial change in this amplitude indicates the presence of an undesired component of $-j_z$ that will shift in the opposite direction as the field is turned on, which leads to unreliability in the value of the extracted Zeeman shift.

In the present calculations for CdSe nanocrystals we find that the conduction electron is primarily *s*-like. In this situation one can identify the effective spin operator **S** with the real spin operator **s**, and hence choose the initial wave function to have a well defined real spin index. We find that the above procedure is extremely stable for calculation of the electron *g* factors, and leads to unambiguous determination of the sign of the *g* factors. The results presented in Sec. III A show that the values for electron *g* factors calculated with this procedure decrease as the nanocrystal size increases. This same trend of a monotonic decrease was also seen in estimates based on effective mass concepts.[2]

In contrast, the hole wave function is primarily *p*-like, as expected for a direct band gap II–VI semiconductor. This renders it difficult to link the effective spin **S** of a hole state to the real spin **s**, resulting in an ambiguity of the sign for the hole *g* factors. In this situation it is more appropriate to express the Zeeman splitting instead by the quadratic form

$$\Delta E^2(\mathbf{B}) \equiv (E(\mathbf{B}) - E(0))^2 = \mu_B^2 \sum_i g_i^2 B_i^2, \qquad (15)$$

in which the sign of the principal *g* factor is not well defined. Typically, the sign convention of the *g* factor in the atomic and bulk limit could then be used as a reference convention to assign a definite sign to the *g* factors in the nanostructure. This is because in both these reference points there usually exists a simple relation between the effective spin operator and real spin operator, which would enable us to determine the corresponding sign of the *g* factor in the nanostructure. However, for bulk CdSe there are to our knowledge no experimental results for electron, hole, and exciton *g* factors. Consequently, in this particular case it is not possible to simply use bulk experimental results as a reference point or guide to determine the sign of the nanocrystal *g* factors. (There do exist experimental results for the related material CdS[7] that will be useful in Sec. III.) In order to assign the signs to the hole *g* factors for CdSe we therefore adopt the following scheme. The hole wave function will be calculated by propagating an initial state that has definite angular momentum indices, e.g., $j=3/2$, $j_z=3/2$, and $j=3/2$, $j_z=1/2$. The sign of the *g* factor is then determined by whether the magnetic field induced energy shift is positive or negative. In the bulk limit this procedure will correctly reproduce the heavy-hole and light-hole values.

A second complication for calculation of the hole *g* factors is the presence of strong mixing between heavy-hole and light-hole components in nanostructures, which is sensitive to both size and shape of the nanostructure. This mixing modifies the corresponding zero-field bases of the two coupled Kramer's doublets and may consequently induce shape and size dependence of the *g* factors for these states. The results presented in Sec. III B below show that for CdSe nanocrystals the hole *g* factor oscillates as a function of size as a result of this heavy-hole/light-hole mixing. We find that calculation of the zero-field *x* and *y* components for the hole states are considerably more affected by this basis mixing than the *z* component, rendering the numerical determination of a zero-field angular momentum eigenstate that adiabatically evolves to a single finite field angular momentum eigenstate more difficult (Sec. III B).

This size and shape dependent mixing of light and heavy hole states presents an additional difficulty for attempting any correlation with atomic and bulk limiting values of hole *g* factors. To our knowledge, there have been no estimates of hole *g* factors for CdSe nanocrystals based on effective mass that may be compared with the present tight-binding results.

D. Gauge invariance

Since in this work the *g* factors will be determined via the energy splitting of the electron and hole states under the external magnetic field, it is essential to cast the tight-binding model into a gauge invariant form. We use the Peierls-coupling tight-binding scheme here to ensure gauge invariance in our tight-binding model.[27–29,33] In this scheme an electromagnetic field specified by the scalar potential $\Phi(\vec{r},t)$ and the vector potential $\mathbf{A}(\vec{r},t)$ will modify the on-site $\langle\alpha,\mathbf{R}_i|H|\alpha,\mathbf{R}_i\rangle$ and off-site $\langle\alpha',\mathbf{R}_i'|H|\alpha,\mathbf{R}_i\rangle$ tight-binding parameters, via

$$\langle\alpha,\mathbf{R}_i|H|\alpha,\mathbf{R}_i\rangle \rightarrow \langle\alpha,\mathbf{R}_i|H|\alpha,\mathbf{R}_i\rangle - \Phi(\mathbf{R}_i,t) \qquad (16)$$

and

$$\langle\alpha',\mathbf{R}_i'|H|\alpha,\mathbf{R}_i\rangle \rightarrow \langle\alpha',\mathbf{R}_i'|H|\alpha,\mathbf{R}_i\rangle e^{-i\frac{e}{\hbar}\int_{R_i}^{R_i'}\vec{A}(\vec{r},t)\cdot d\vec{l}}, \qquad (17)$$

where a straight line should be taken for the integral over the vector potential.

To impose gauge invariance, we thus only need to modify the tight-binding hopping constant (transfer integral) between nearest neighbors. Since there are only seven independent hopping directions in a wurtzite structure, the gauge phase can be calculated and stored before performing the time propagation. A brief summary of the gauge phase in the wurtzite structure is given in the appendix.

To estimate the contribution to the Zeeman splitting that derives from the gauge phase, we have calculated the Zeeman splitting without gauge phase for some of the nanocrystals studied here. We find that the gauge phase is responsible

TABLE I. Size, diameters, and aspect ratio of the nanostructures.

Number of atoms	66	108	144	237	336	384	450	561	758	768	777	1501
$\sqrt{L_xL_y}$(Å)	13.38	13.38	16.92	21.85	21.85	25.39	26.76	22.85	34.55	27.42	20.44	43.01
L_z(Å)	11.38	18.38	18.38	14.88	21.88	24.38	21.88	35.88	35.88	39.38	49.88	42.88
Aspect ratio	0.85	1.37	1.09	0.68	1.00	0.99	0.82	1.64	1.04	1.44	2.44	0.99

for 10%–40% of the Zeeman energy. Without the gauge phase the Zeeman splitting increases and becomes more isotropic.

III. RESULTS

We investigate CdSe nanostructures having 66–1501 atoms. This roughly corresponds to the size range of 15–43 Å in effective diameter. In our calculation we define the aspect ratio to be the ratio between effective in-plane diameter ($\sqrt{L_xL_y}$) and out-of-plane diameter (L_z). The aspect ratio of these nanostructures ranges from 0.68 to 1.64. These can be divided into three different aspect ratio groups. The first group has aspect ratio well below one, ranging from 0.68 to 0.85. The second group has aspect ratio approximately equal to one, ranging from 0.99 to 1.09. The third group has aspect ratio well above one, ranging from 1.37 to 1.64. A nanostructure with aspect ratio 2.44 is also studied, in order to probe the trends of g factors in the quantum rod limit. In Table I we summarize the in-plane diameter and out-of-plane diameter values of the nanostructures. If the aspect ratio of the nanostructures deviates from 1.0 by less than 10% then it is appropriate to use a single effective diameter ($\sqrt{L_xL_yL_z}$) to characterize the nanostructure. Note that the nanostructures used in TRFR experiments to date[2] have reported aspect ratios in the range of 1.17–1.34. However, a single effective diameter was, nevertheless, used to characterize the nanostructures. Furthermore, the TRFR sample possessed a 5%–15% size distribution and ±0.2 aspect ratio variation. Hence, one must be cautious when making a quantitative comparison between the calculated and the experimental results.

To verify that the tight-binding model can reproduce the general features of conduction band, valence band, and identifiable band gap for nanostructures we have calculated the total density of states (TDOS) for smaller nanostructures (66–450 atoms). In Fig. 1 we plot the low resolution (≈50 meV) TDOS for a 450 atom CdSe nanostructure. It is evident from the figure that the conduction band edge (CBE), valence band edge (VBE), and band gap can be easily identified. It should be noted that the TDOS calculation is computationally expensive because one has to sum over a complete set of initial states. However, only the states at the band edges are relevant to the optical orientation experiment. A prior knowledge of the TDOS is not necessary for calculation of the band edge eigenstates. A reasonable initial guess of the band edge eigenenergy is sufficient for calculation of high resolution band edge eigenenergies and eigenfunctions through an iterative procedure described below. For the smaller nanostructures where we have calculated the TDOS, we use the band edge energies identified from the TDOS data as initial values. For the larger nanostructures, we assign the initial value of band edge energies by extrapolating the band edge energies of the smaller nanostructures.

To get the high resolution band edge eigenenergies and eigenstates we first estimate the eigenenergies as described above. A low resolution eigenstate is then generated using some judiciously chosen initial state. The initial state is set up to have nonzero overlap with the desired eigenfunction and to possess a well-defined value of some particular quantum number such as the z component of the local total angular momentum, j_z. This low resolution eigenstate is then put through the spectral weight analysis described in Sec. II B which results in a higher resolution eigenenergy. The higher resolution eigenenergy is then used together with the lower resolution eigenstate to generate a higher resolution eigenstate. This process is iterated until the desired accuracy is acquired and, in the case of the hole, until the near degeneracy between heavy-hole-like and light-hole-like doublets is lifted. Once the CBE and VBE eigenenergies are found, the band gap can be trivially calculated from $E_{\text{gap}}=E_{\text{CBE}}-E_{\text{VBE}}$. In Fig. 2 we plot the high resolution results for the size dependent CBE energy, VBE energy, and band gap. These results are all stable with respect to further iteration. Note that the VBE consists of two nearly degenerate Kramer's doublets. As the size of the nanostructure increases, these two doublets will converge, respectively, to the heavy and light hole doublets in bulk CdSe.

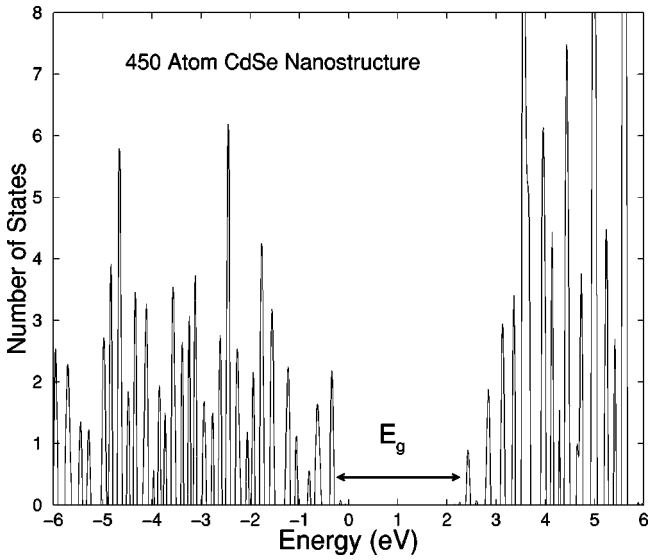

FIG. 1. Total density of states for a 450 atom CdSe nanocrystal.

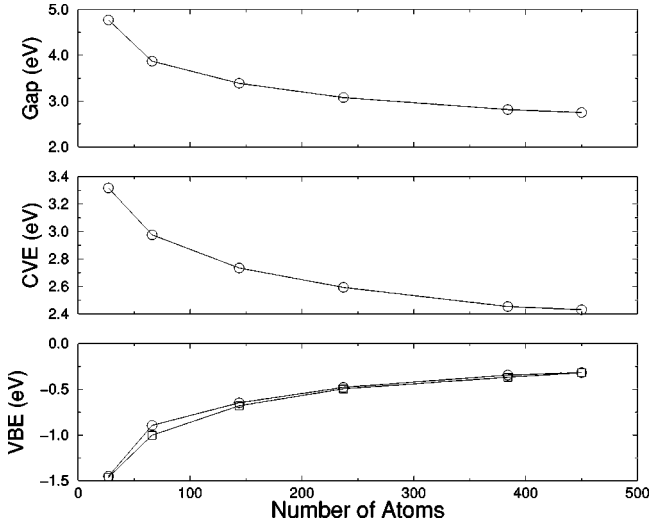

FIG. 2. (a) Band gap (b) CBE energy (c) VBE energy as a function of the number of atoms. Note that the VBE consists of two nearly degenerate levels in a CdSe nanocrystal, each corresponding to a perturbed Kramer's doublet, i.e., four states in total.

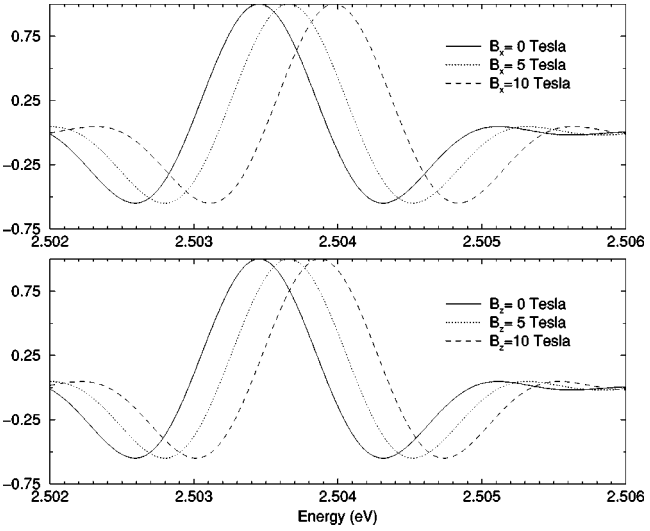

FIG. 3. Zeeman shift of the $|\Psi^{+x}\rangle$ component of the Kramer's doublet in the CBE when (a) the external field B is in the $+x$ direction and (b) the $+z$ direction.

A. Electron *g* factor

Although the CdSe nanostructures we studied here have only approximate C_{3v} symmetry, we expect, nevertheless, that the principal axes are still located approximately along the x, y, and z directions. This is supported by the result of a perturbative time-independent tight-binding calculation of g factors for these same nanocrystals[6] in which it was found that $g_x \approx g_y \neq g_z$. As described in Sec. II C, to accurately identify the Zeeman splitting it is necessary to generate the Kramer's doublet which will evolve into the Zeeman eigenstates when we turn on the external magnetic field. For the CBE states, the Kramer's doublet $|\psi^{\pm z}\rangle$ for a magnetic field pointing in the $+z$-direction can be generated via setting all local orbitals of the initial states to have spin equal to $\pm 1/2$. The Kramer's doublet for x and y directions are then obtained as $|\psi^{\pm x}\rangle = \frac{1}{\sqrt{2}}(|\psi^{+z}\rangle \pm |\psi^{-z}\rangle)$ and $|\psi^{\pm y}\rangle = \frac{1}{\sqrt{2}}(|\psi^{+z}\rangle \pm i|\psi^{-z}\rangle)$, respectively. The external magnetic field is limited to be less than 10 T, which corresponds to the range of magnetic field in the typical experiments.[2,3] To make the connection to the CBE in the bulk material, which is s-like, we calculate the spectral weight of the $|s, \sigma = 1/2\rangle$ local orbitals of Cd and Se in the state $|\psi^{+z}\rangle$. In Table II we summarize the size dependence of these s-orbital spectral weights. We find that the CBE electron in the nanostructure is still primarily s-like, with spectral weights greater than 0.75 for all sizes. The s-orbital contribution increases monotonically as the size increases.

In Fig. 3 we plot the magnetic field dependent spectra for the $|\psi^{+x}\rangle$ state with magnetic field in the x direction and for the $|\psi^{+z}\rangle$ state with magnetic field in the z direction, for a 336 atom CdSe nanocrystal. Assuming the spectral peaks have line shapes of the form $\mathcal{L}(E - E_n(B))$, the magnetic field dependent eigenenergy $E_n(B)$ can then be determined with very high accuracy. The g factor is then extracted by fitting $E_n(B)$ as a function of B.

Figure 4 shows the resulting electron g factors as a function of the length parameter L_z. The data are grouped according to the aspect ratio of the nanostructure. Group 1 (down triangles) has aspect ratio 0.68–0.85, group 2 (open squares) has aspect ratio 0.99–1.09, and group 3 (up triangles) has aspect ratio 1.37–1.64. One calculation for a nanocrystal with aspect ratio 2.44 is also included (closed circle). The g factor values derived from TRFR experiments on similar size CdSe nanocrystals[2] are also plotted for comparison (asterisks). The 5%–15% size distribution of the experimental sample is represented in the figure by the horizontal error bar. As noted above, the aspect ratio of the sample in TRFR experiment in this size range was estimated as 1.17–1.34, with a ±0.2 variation. The present calculations yield $g_x \simeq g_y > g_z$, where equality is within the resolution for all nanocrystals, as expected for structures possessing approximate C_{3v} symmetry. As a result, only two sets of data are shown in the figure and the average value $g_\perp = (g_x + g_y)/2$ is used to represent both g_x and g_y, where the notation $g_\perp$ refers to the response to a field perpendicular to the hexagonal (c) axis of the nanocrystal.

Similar to Ref. 6, these results show a strong shape dependence of the electron g factor. However, these nonperturbative results show stronger anisotropy compared to the perturbative results of Ref. 6 and also a qualitatively different

TABLE II. Spectral weights of the $|s, \sigma = 1/2\rangle$ local orbitals of Cd and Se in the state $|\psi^{+z}\rangle$.

Number of atoms	66	108	143	237	336	384	450	561	758	768	777	1501
$\lvert s, \sigma = \frac{1}{2}\rangle$	0.75	0.79	0.81	0.83	0.85	0.86	0.86	0.88	0.87	0.88	0.89	0.90

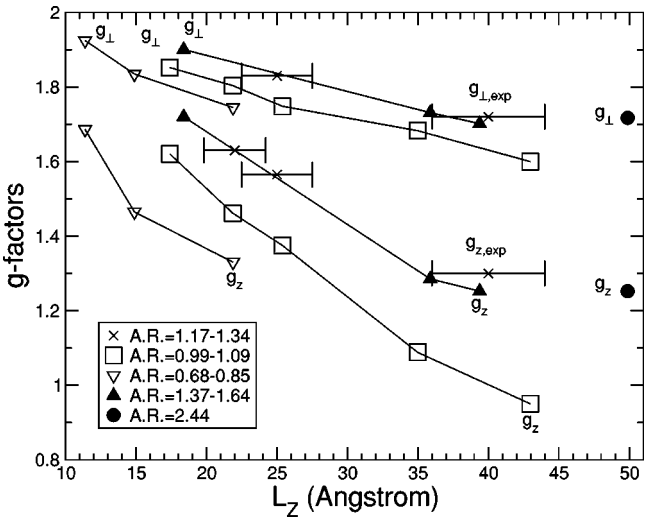

FIG. 4. CdSe nanocrystal electron g factors as a function of the nanocrystal length parameter L_z. The term g_z corresponds to the magnetic response along the hexagonal crystal axis, and $g_\perp$ refers to the average of g_x and g_y. Crosses denote experimental values from Ref. 2, all other symbols refer to the present nonperturbative tight-binding calculations. The closed triangles show the calculated values lying closest to the experimental results, which correspond to aspect ratios 1.37–1.64, in good agreement with the aspect ratios of the experimental sample.

aspect ratio dependence. This latter point will be addressed in more detail below. Both g factors g_z and $g_\perp$ decrease monotonically as a function of the nanocrystal size. The value of g_z decreases rapidly, while the value of $g_\perp$ decreases more gradually. We note that under certain growth conditions it is possible to synthesis CdSe nanostructures with zinc blende structure.[31] It is expected that for zinc blende CdSe nanocrystals, if the shape of the nanostructure also has high symmetry, there will be only one isotropic g factor component.[32]

Figure 4 shows a good agreement between the current calculations and the experimentally measured pairs of g factor values over this size range. We note that due to variable orientations of the nanocrystal in the TRFR experiments of Ref. 2, quantitative comparison with the TRFR g factors requires making an average over allowed nanocrystal orientations in order to obtain a time-dependent spin magnetization to which empirical g factors could be fit.[30] Detailed comparison would require microscopic knowledge of the matrix environment of the nanocrystals, which is unfortunately not well understood. Thus it is not clear to what extent the anisotropy of the electron g factors predicted here for single nanocrystals will be reflected in an ensemble measurement. The quantitative agreement between theory and experiment in Fig. 4 is sufficiently striking that it appears possible that the two experimentally observed distinct g factor values might derive from the electronic values $g_\perp$ and g_z, even after some averaging over nanocrystal orientations. We note that the theoretical description of the nanocrystals employed here provides a realistic representation of the nanocrystal shape that is consistent with detailed transmission electron microscopy analyses of the nanocrystals used for the TRFR experiments in Ref. 2. This interpretation of observation of multiple g factors deriving from an electron g factor anisotropy that is dependent on the shape and size of the CdSe nanocrystals is different from the original experimental speculation that one of the observed g factors might be identified with an isotropic electron g factor while the other g factor might be identified with an exciton g factor.[2]

It is intriguing to look into the aspect ratio dependence of the g factors in more detail. We observe from Fig. 4 that both $g_\perp$ and g_z increase as the aspect ratio increases, provided that the aspect ratio is less than 1.64. We find that g_z is more sensitive to the aspect ratio and increases much more with this than $g_\perp$. The g factors begin to saturate between aspect ratio 1.64 and 2.44. It is expected that if one continues to increase the aspect ratio then g_z should begin to decrease, since it eventually should approach the bulk value. On the other hand, $g_\perp$ should stay roughly constant after it saturates, provided that the in-plane cross section is kept the same when one increases the aspect ratio. It should be emphasized that the aspect ratio is only a simple indicator for the shape of the nanostructure. Two nanostructures with similar number of atoms and aspect ratio values might still have very different shape or surface structure. From the observations above it is clear that we can identify a range of aspect ratios in which the effect of anisotropy of the wurtzite structure and that of the shape of the nanocrystal partially cancel each other so that the electron g factors become more isotropic. In the cases studied here it appears that the cancellation is not complete. It also appears unlikely from these exact calculation of g factors that the cancellation will become more complete for large-size nanocrystals, since the difference between g_z and $g_\perp$ increases for larger nanocrystals having aspect ratio approximately unity. As a result, a true quasispherical regime as predicted by an analysis perturbative in spin[6,13] in which the electron g factors become isotropic may never be reached.

B. Hole g factor

We have calculated the hole g factors for the two nearly degenerate valence band edge doublets, which will be denoted by h_1 and h_2. We define h_1 and h_2 to be the highest and second highest energy valence band states, respectively. In the bulk limit, the energy difference of these states corresponds to the A-B splitting of the semiconductor. To connect the h_1 and h_2 states to the heavy and light hole states in the bulk material we calculate the spectral weights of local orbitals possessing definite angular momentum quantum number $|j=\frac{3}{2},j_z\rangle$ in h_1 and h_2. These spectral weights are summarized in Tables III and IV.

We find that for nanocrystals in the size range we are interested in, the mixing between the $\pm 3/2$ and $\pm 1/2$ components is very strong. The mixing appears to be sensitive to the size of the nanocrystal, without any clear trend emerging. We attribute this is to an additional sensitivity to nanocrystal shape which is coupled with size for these atomistic representations of nanocrystals, as discussed elsewhere.[6] As a result of this mixing it becomes improper to rigorously identify the $h_1(h_2)$ state with the heavy (light)-hole states, respectively.

TABLE III. Spectral weights of the local orbitals $|j=3/2, j_z\rangle$ in the h_1 state.

Number of atoms	66	108	144	237	336	384	450	561	758	768	777	1501
$j_z=+\frac{3}{2}$	0.47	0.03	0.27	0.82	0.06	0.30	0.81	0.06	0.87	0.37	0.51	0.88
$j_z=+\frac{1}{2}$	0.12	0.78	0.24	0.02	0.78	0.21	0.03	0.79	0.02	0.11	0.34	0.03
$j_z=-\frac{1}{2}$	0.29	0.00	0.37	0.04	0.04	0.39	0.06	0.05	0.04	0.18	0.02	0.04
$j_z=-\frac{3}{2}$	0.01	0.03	0.02	0.00	0.04	0.02	0.02	0.02	0.00	0.25	0.00	0.00

For each nanocrystal we first look at the spectral weight of h_1 and h_2 states and determine which is more heavy hole-like. Then to find the best zero-magnetic field eigenstate in the twofold degenerate space spanned by the corresponding Kramer's doublet, we proceed as follows: $|\psi^{\pm z}\rangle$ is generated by setting initially all local orbitals to have $j=3/2$, $j_z=\pm 3/2$ or $j=3/2$, $j_z=\pm 1/2$ and $|\psi^{\pm x}\rangle$ is generated by setting initially all local orbitals to have $j=3/2$, $j_x=\pm 3/2$ or $j=3/2$, $j_x=\pm 1/2$. The g factor is extracted from the finite field Zeeman shifts by setting $m=1$ in Eq. (12). This defines the numerical scale of the g factors for heavy- and light-hole-like states to be equal, which is the preferred convention when there is strong mixing of these states (see discussion below). As described in Sec. II C. above, the quality of the zero-magnetic field eigenvector can be checked by examining the amplitude of the spectral peak resulting from this initial state. Thus, if the peak amplitude remains very close to 1.0 when the magnetic field is turned on, then it is a valid zero-magnetic field eigenvector. However, if the peak amplitude deviates from 1.0, it indicates that the initial eigenvector contains components of zero-magnetic field eigenvectors that will shift in opposite directions when the external magnetic field is turned on and the resulting spectrum is the sum of two line shape functions whose centers differ by the Zeeman energy splitting. In this case, the Zeeman energy cannot be reliably extracted from the spectra. Of the nanocrystals studied in this work, we find that $|\psi^x\rangle$ of light-hole-like states for nanocrystals with 450, 777, and 1501 atoms fail to generate a reliable zero-magnetic field eigenstate. As discussed earlier, this is due to the large degree of mixing between the heavy-hole and light-hole-like states.

In Fig. 5 and Fig. 6 we plot the size-dependent hole g factors for the two hole doublets. The data has been grouped into heavy-hole-like and light-hole light states. Similarly to the electron g factors, the data for hole g factors for these sizes are also grouped by the nanocrystal aspect ratio. We find that for the heavy-hole-like state, $g_\perp$ is close to zero except for the smallest nanocrystal for which it remains finite. For the heavy-hole like states the parallel component g_z shows a similar same aspect ratio dependence as the electron g factors, but in addition the heavy-hole-like g_z also shows some oscillation as a function of nanocrystal size. For the light-hole-like states, we observe oscillations for both $g_\perp$ and g_z, but the general trend is not as clear as for the heavy-hole-like states.

It is important to clarify how these g factors should approach the relevant bulk values when the size of the nanocrystal increases further. In the bulk CdSe semiconductor, the valence band near the Γ point can be described by the Luttinger Hamiltonian.[35] The states $|3/2, \pm 3/2\rangle$ and $|3/2, \pm 1/2\rangle$ are associated with the heavy hole and light hole, respectively. If the heavy hole and light hole are really degenerate, then Eq. (11) is not actually appropriate, since then the full fourfold nature of the $j=3/2$ angular momentum state has to be taken into account. When the heavy-hole and light-hole states are not degenerate and the mixing between $|3/2, \pm 1/2\rangle$ and $|3/2, \pm 3/2\rangle$ components is small, then one can use Eq. (11) and set $m=3$ for the heavy hole and $m=1$ for the light hole in Eq. (12). However, when this mixing is strong, as in the nanocrystals studied here, it is preferable to use a single value of m for both states to facilitate comparison. We now consider the relation of the hole g factors in Figs. 5 and 6 to the corresponding bulk values. The finding that $g_\perp$ for the heavy-hole-like state is close to zero for all except the smallest size nanocrystals is consistent with analysis of the Luttinger Hamiltonian. It can readily be shown from the form of this that $g_\perp$ is negligible if the heavy-hole/light-hole mixing and the k^3 terms are neglected. Thus the hole value of $g_\perp$ appears to rapidly approach the expected bulk value predicted by the Luttinger Hamiltonian as the nanocrystal size increases. Although the hole g factor has not been measured for bulk CdSe, experimental measurements for the related material CdS show that $g_\perp$ is zero for CdS in the hexagonal structure[7] and it is reasonable to expect a similar value for CdSe.

We attribute the oscillations in the hole g factors with nanocrystal size to the irregular mixing of local orbitals evident in Tables III and IV as a function of nanocrystal size. From Table III we observe that the h_1 state becomes increasingly heavy-hole-like for nanocrystals having more than 450

TABLE IV. Spectral weights of local orbitals $|j=3/2, j_z\rangle$ in the h_2 state.

Number of atoms	66	108	144	237	336	384	450	561	758	768	777	1501
$j_z=+\frac{3}{2}$	0.02	0.46	0.04	0.46	0.64	0.40	0.36	0.53	0.37	0.37	0.35	0.04
$j_z=+\frac{1}{2}$	0.06	0.20	0.03	0.03	0.10	0.13	0.13	0.33	0.17	0.11	0.10	0.83
$j_z=-\frac{1}{2}$	0.08	0.13	0.37	0.35	0.09	0.17	0.41	0.02	0.37	0.19	0.43	0.02
$j_z=-\frac{3}{2}$	0.68	0.07	0.43	0.00	0.08	0.22	0.01	0.01	0.01	0.23	0.06	0.06

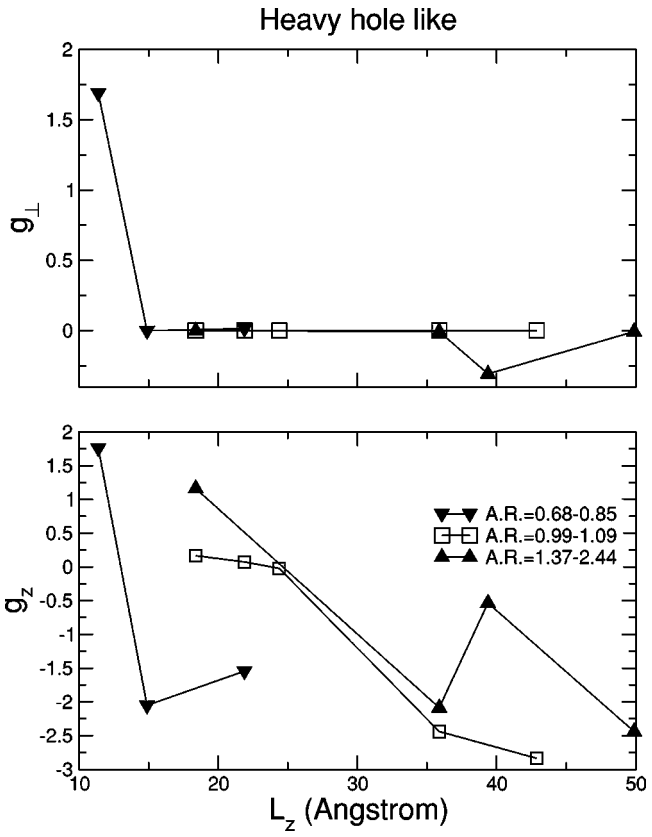

FIG. 5. CdSe nanocrystal heavy-hole-like hole g factors as a function of the nanocrystal length parameter L_z. A.R. denotes the nanocrystal aspect ratio, g_z refers to the component parallel to the hexagonal crystal axis, and $g_\perp$ to the component perpendicular to this.

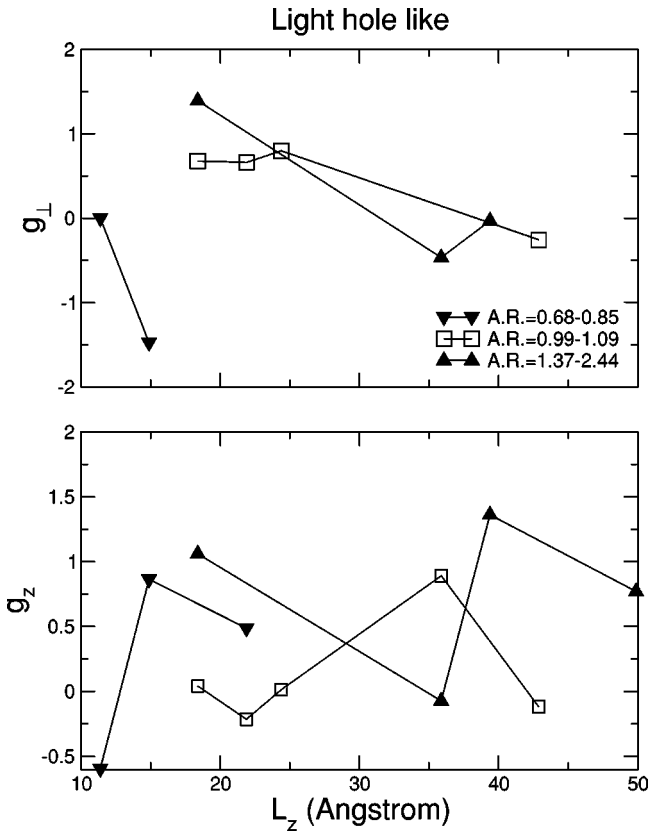

FIG. 6. CdSe nanocrystal light-hole-like hole g factors as a function of the nanocrystal length parameter L_z. A.R. denotes the nanocrystal aspect ratio, g_z refers to the component parallel to the hexagonal crystal axis, and $g_\perp$ to the component perpendicular to this.

atoms, provided that the aspect ratio is close to one. It is expected that as the size of the nanocrystal increases further, the two hole states will eventually converge to the heavy-hole and light-hole states, respectively. One must then be careful when comparing the hole g factor values calculated for finite nanocrystals by the present method with the bulk heavy-hole g factor, since as noted above the latter is usually defined with $m=3$ in Eq. (12),[14] while the value of m in this work is set to 1 for all hole states because of the strong mixing between light-hole-like and heavy-hole-like states (see above).

This evidence of mixing between the heavy- and light-hole states, and its sensitivity to the nanocrystal size and shape also implies that an exciton in a nanostructure within this size range cannot be simply considered as a sum of electron and heavy-hole or light-hole states. The exciton g factor will therefore also be sensitive to the size and shape of the nanocrystal.

IV. SUMMARY AND DISCUSSION

We have calculated the g factors of the conduction band edge electrons and valence band edge holes in CdSe nanostructures using the time-dependent tight-binding method and a finite field approach to the evaluation of the g factors. This approach allows an exact, nonperturbative analysis, with high resolution of the Zeeman shifts for both electrons and holes.

Application to CdSe nanocrystals of variable shape and size that simulate the experimentally accessible wurtzite CdSe nanocrystals showed that the electron g factor is strongly anisotropic in these systems. In particular, we find that $g_x \simeq g_y > g_z$ for all nanocrystal sizes, where z denotes the wurtzite axis. This is consistent with the approximate C_{3v} symmetry of the nanocrystals. The magnitude of the anisotropy splitting is seen to increase for larger nanocrystals, while each of the g factor components decreases with increasing nanocrystal size. The strong g factor anisotropy seen here in these nonperturbative calculations provides confirmation of the qualitative predictions of size-dependent anisotropy in electron g factors seen in the perturbative calculations of Ref. 6. However, the nonperturbative calculations now provide quantitatively accurate values for the components of the g tensor, unlike the previous perturbative analysis. This improvement derives from the nonperturbative treatment of the spin-orbit interaction, which is relatively strong compared to the effect of the external magnetic field and which should therefore be treated nonperturbatively if possible.

We have investigated the dependence of the electron g factors on the nanocrystal aspect ratio in considerable detail.

We find that in general the g factors initially increase as a function of the aspect ratio, and that g_z increases more than $g_\perp$. The increase of g factors saturates around a value of aspect ratio 1.62–2.44. It is expected that g_z would then begin to decrease again until it reaches the bulk value while $g_\perp$ would stay roughly the same, if the aspect ratio were to continue to increase further. The observed aspect ratio dependence allows us to identify a regime where the anisotropy derived from the wurtzite structure and that derived from the shape of the nanocrystal partially cancel each other, resulting a more isotropic regime. However, a full cancellation is never reached in the present calculations, unlike the previous perturbative tight-binding analysis where a complete cancellation over a finite size range was seen.[6] From the present nonperturbative calculations it also appears unlikely that in larger nanocrystals the cancellation would become complete, since the difference between g_z and $g_\perp$ for a unit aspect ratio nanocrystal is seen to increase as a function of the nanocrystal size.

Unlike the perturbative approach, the time-dependent approach allows direct calculation of hole g factors, despite complications due to the valence band degeneracies which require projecting out initial states of specific total angular momentum and of its z projection. We find that the valence band edge for these size nanocrystals consists of two nearly degenerate Kramer's doublets that may be assigned to pairs of light-hole-like and heavy-hole-like states, respectively. However, this assignment should be understood as an approximation, due to the strong heavy-hole/light-hole mixing. The hole g factors for these states can be calculated once projections onto well-defined states of j and j_z are established. We find that the value of $g_\perp$ for the heavy-hole-like states is mostly close to zero, which is consistent with analysis of the Luttinger Hamiltonian for bulk and with measurements for the related material CdS in the bulk. All other hole g factor components show marked oscillations as a function of the nanocrystal size. This is attributed to a strong, size-dependent mixing of the two pairs of hole states deriving from light- and heavy-hole pairs. For g_z, the aspect ratio dependence of heavy-hole-like states behaves similarly to that for the electron g factor g_z, although the superimposed oscillations make it more difficult to describe the general trend for the holes.

These results have implications for the g factors of excitons, namely of electron-hole pairs correlated by the Coulomb interaction. The g factor of an uncorrelated electron-hole pair may be approximated by $g_x=g_e-g_h$. The mixing between the heavy- and light-hole states, and sensitivity to the nanocrystal size and shape, implies that an exciton in this size range cannot be simply considered as a sum of electron and heavy-hole or electron and light-hole states. The exciton g factor must therefore also be sensitive to the size and shape of the nanocrystal. In addition, the Coulomb interaction can also be expected to modify the simple sum of electron and hole contributions. As discussed above, it appears feasible to extend the current scheme to now calculate the corresponding exciton g factors, although this would not be possible with a standard time-independent approach based on direct diagonalization. Since the exciton fine structure splitting in CdSe nanocrystal is of the order 1–10 meV[21] the energy resolution obtained here ($\approx 1\ \mu$V) appears to be sufficient to resolve the exciton fine structure.

Finally, we note that the size dependence of the anisotropic electron g factors $g_\perp$ and g_z shows quantitative agreement with the pairs of values extracted from TRFR experimental data over the same size range of nanocrystals. While some averaging over nanocrystal orientation would be required in order to make unambiguous comparison with the experimental observations, it appears possible that the two distinct g factors seen in the TRFR experiments may be derived from the two components g_z and $g_\perp$ of the electron g factor. This provides a different interpretation from the earlier speculations that one of the observed g factors is an isotropic electron g factor while the other one should be assigned to an exciton g factor.[2] In this context, extension of the current calculation scheme to the evaluation of exciton g factors in these nanostructures would be extremely desirable and interesting, particularly since the only existing estimate for an exciton g factor relies upon a free parametrization of the hole contribution.[2]

ACKNOWLEDGMENTS

The authors acknowledge the financial support by DARPA and ONR under Grant No. FDN0014-01-1-0826 and by the ARO under Grant No. FDDAAD19-01-1-0612. We thank NPACI for a generous allocation of supercomputer time at the San Diego Supercomputer Center. We also thank Dr. Seungwon Lee and Josh Schrier for fruitful discussions.

APPENDIX

In the wurtzite structure there are seven independent electron hopping directions. In this calculation these seven hopping directions are denoted by $\vec{d}_p$, $p=1\ldots7$, and are assigned to be the following vectors:

$$\vec{d}_1 = \tfrac{a_0}{3}(0,0,3),$$

$$\vec{d}_2 = \tfrac{a_0}{3}(2\sqrt{2},0,-1),\ \vec{d}_5 = \tfrac{a_0}{3}(-2\sqrt{2},0,-1),$$

$$\vec{d}_3 = \tfrac{a_0}{3}(-\sqrt{2},\sqrt{6},-1),\ \vec{d}_6 = \tfrac{a_0}{3}(\sqrt{2},-\sqrt{6},-1),$$

$$\vec{d}_4 = \tfrac{a_0}{3}(-\sqrt{2},-\sqrt{6},-1),\ \vec{d}_7 = \tfrac{a_0}{3}(\sqrt{2},\sqrt{6},-1). \qquad \text{(A1)}$$

Here $a_0=2.625$ Å is the lattice constant. This convention enables us to calculate the gauge-dependent quantities explicitly.

For a fixed external magnetic field $\vec{B}=(B_x,B_y,B_z)$ we assign the vector potential to be $\vec{A}=\frac{1}{2}\vec{B}\times\vec{r}$. We define a magnetic-field-dependent gauge phase

$$\phi(\vec{R}_a,\vec{d}_{\rm dir}) = \frac{e}{\hbar}\int_{\vec{R}_a}^{\vec{R}_a+\vec{d}_{\rm dir}} \vec{A}\cdot\vec{dl}, \qquad \text{(A2)}$$

where $\vec{R}_a$ represents the position vector of an anion. The gauge phase for the cation can be easily calculated by taking the appropriate complex conjugation of the phase of the cor-

responding anion. With the line of integration taken to be a straight line, the integral can be calculated analytically. We denote $|\Psi\rangle$ to be the wave function of the system and $|\Psi_\ell(\vec{R}_a)\rangle$ ($|\Psi_m(\vec{R}_c)\rangle$) to be the tight-binding local l (m)-orbital wave functions for an anion (cation) located at $\vec{R}_a$ ($\vec{R}_c$) where $\vec{R}_a$ and $\vec{R}_c$ are nearest neighbors. Let $A_\ell = \langle\Psi|\Psi_\ell(\vec{R}_a)\rangle$ and $A_m = \langle\Psi|\Psi_\ell(\vec{R}_c)\rangle$.

Using this notation the gauge-dependent short-time propagation of the electron hopping in some particular direction becomes

$$\begin{aligned} e^{-\hat{V}_{\ell m,\mathrm{dir}}dt}(A_l|\Psi_l(\vec{R}_a)\rangle + A_m|\Psi_m(\vec{R}_c)\rangle) \\ = (A_\ell \cos(V_{\ell m}dt) - iA_m \sin(V_{\ell m}dt)e^{+i\phi(\vec{R}_a,\vec{d}_{\mathrm{dir}})})|\Psi_l(\vec{R}_a)\rangle \\ + (A_m \cos(V_{\ell m}dt) - iA_\ell \sin(V_{\ell m}dt)e^{-i\phi(\vec{R}_a,\vec{d}_{\mathrm{dir}})})|\Psi_m(\vec{R}_c)\rangle, \end{aligned} \tag{A3}$$

where $V_{\ell m}$ is the hopping constant (transfer integral) in zero magnetic field.

[1] D. K. Young *et al.*, Semicond. Sci. Technol. **17**, 275 (2002).
[2] J. A. Gupta, D. D. Awschalom, Al. L. Efros, and A. V. Rodina, Phys. Rev. B **66**, 125307 (2002).
[3] J. A. Gupta, D. D. Awschalom, X. Peng, and A. P. Alivisatos, Phys. Rev. B **59**, R10421 (1999).
[4] M. Kuno, M. Nirmal, M. G. Bawendi, A. L. Efros, and M. Rosen, J. Chem. Phys. **108**, 4242 (1998).
[5] A. V. Kadavanich, Ph.D. thesis, University of California, Berkeley, 1997.
[6] J. Schrier and K. B. Whaley, Phys. Rev. B **67** 235301 (2003).
[7] D. G. Thomas and J. J. Hopfield, Phys. Rev. **175**, 1021 (1968).
[8] D. J. Hilton and C. L. Tang, Phys. Rev. Lett. **89**, 146601 (2002).
[9] T. Uenoyama and L. J. Sham, Phys. Rev. Lett. **64**, 3070 (1990).
[10] M. Paillard, X. Marie, P. Renucci, T. Amand, A. Jbeli, and J. M. Girard, Phys. Rev. Lett. **86**, 1634 (2001).
[11] A. A. Kiselev, E. L. Ivchenko, and U. Rössler, Phys. Rev. B **58**, 16353 (1998).
[12] A. V. Rodina, Al. L. Efros, M. Rosen, and B. K. Meyer, Mater. Sci. Eng., C **19**, 435 (2002).
[13] A. V. Rodina, Al. L. Efros, and A. Yu. Alekseev, Phys. Rev. B **67**, 155312 (2003).
[14] A. V. Nenashev, A. V. Dvurechenskii, and A. F. Zinovieva, Phys. Rev. B **67**, 205301 (2003).
[15] A. J. Stone, Proc. R. Soc. London, Ser. A **271**, 424 (1963).
[16] N. A. Hill and K. B. Whaley, Chem. Phys. **210**, 117 (1996).
[17] K. Leung and K. B. Whaley, Phys. Rev. B **56**, 7455 (1997).
[18] S. Pokrant and K. B. Whaley, Eur. Phys. J. D **6**, 255 (1999); S. Pokrant, Diplomarbeit, Phillips-Universität Marburg, Marburg, 1996.
[19] P. E. Lippens and M. Lannoo, Phys. Rev. B **41**, 6079 (1990).
[20] J. J. Shiang, A. V. Kadavanich, R. K. Grubbs, and A. P. Alivisatos, J. Phys. Chem. **99**, 17417 (1995).
[21] K. Leung, S. Pokrant, and K. B. Whaley, Phys. Rev. B **57**, 12291 (1998).
[22] N. A. Hill and K. B. Whaley, Phys. Rev. Lett. **75**, 1130 (1995).
[23] S. Lee *et al.*, J. Computational Electron. (in press).
[24] M. D. Feit, J. A. Fleck, Jr., and A. Steiger, J. Comput. Phys. **47**, 412 (1982).
[25] J. J. Sakurai, *Modern Quantum Mechanics* (Addison–Wesley, Reading, MA, 1994).
[26] M. Suzuki, Prog. Theor. Phys. **56** 1454 (1976).
[27] M. Graf and P. Vogl, Phys. Rev. B **51**, 4940 (1995).
[28] T. B. Boykin, R. C. Bowen, and G. Klimeck, Phys. Rev. B **63**, 245314 (2001).
[29] T. B. Boykin and P. Vogl, Phys. Rev. B **65**, 035202 (2001).
[30] J. A. Gupta, Ph.D dissertation, University of California, Santa Barbara, 2002.
[31] L. Manna, E. C. Scher, and A. P. Alivisatos, J. Cluster Sci. **13**, 521 (2002).
[32] S. Lee and K. B. Whaley (unpublished).
[33] B. A. Foreman, Phys. Rev. B **66**, 165212 (2002).
[34] D. J. Chadi, Phys. Rev. B **16**, 790 (1977).
[35] J. M. Luttinger, Phys. Rev. **102**, 1030 (1955).